

## Article

# Carbon-Based FET-Type Gas Sensor for the Detection of ppb-Level Benzene at Room Temperature

Risheng Cao <sup>1</sup>, Zhengyu Lu <sup>1</sup>, Jinyong Hu <sup>1,\*</sup> and Yong Zhang <sup>1,2,\*</sup> 

<sup>1</sup> School of Physics and Optoelectronics, Xiangtan University, Xiangtan 411105, China; caorisheng96@163.com (R.C.); zhengyu990428@163.com (Z.L.)

<sup>2</sup> Hunan Institute of Advanced Sensing and Information Technology, Xiangtan University, Xiangtan 411105, China

\* Correspondence: jyhu\_233@xtu.edu.cn (J.H.); zhangyong@xtu.edu.cn (Y.Z.)

**Abstract:** Benzene, as a typical toxic gas and carcinogen, is an important detection object in the field of environmental monitoring. However, it remains challenging for the conventional resistance-type gas sensor to effectively detect low-concentration (ppb-level) benzene gas molecules, owing to their insufficient reaction activation energy, especially when operating at room temperature. Herein, a field-effect transistor (FET)-type gas sensor using carbon nanotubes as a channel material is proposed for the efficient detection of trace benzene, where carbon nanotubes (CNTs) with high semiconductor purity act as the main channel material, and ZnO/WS<sub>2</sub> nanocomposites serve as the gate sensitive material. On the basis of the remarkable amplification effect in CNTs-based FET, the proposed gas sensor manifests desirable sensitive ability with the detection limit as low as 500 ppb for benzene even working at room temperature, and the sensor also exhibits fast response speed (90 s), high consistency with a response deviation of less than 5%, and long-term stability of up to 30 days. Furthermore, utilizing Tenax TA as the screening unit, the as-proposed gas sensor can achieve the feasible selective detection of benzene. These experimental results demonstrate that the strategy proposed here can provide significant guidance for the development of high-performance gas sensors to detect trace benzene gas at room temperature.

**Keywords:** CNTs-based FET gas sensor; ZnO/WS<sub>2</sub> nanocomposites; ppb-level benzene detection; Tenax TA screening unit



**Citation:** Cao, R.; Lu, Z.; Hu, J.; Zhang, Y. Carbon-Based FET-Type Gas Sensor for the Detection of ppb-Level Benzene at Room Temperature. *Chemosensors* **2024**, *12*, 179. <https://doi.org/10.3390/chemosensors12090179>

Received: 28 July 2024

Revised: 29 August 2024

Accepted: 3 September 2024

Published: 4 September 2024



**Copyright:** © 2024 by the authors. Licensee MDPI, Basel, Switzerland. This article is an open access article distributed under the terms and conditions of the Creative Commons Attribution (CC BY) license (<https://creativecommons.org/licenses/by/4.0/>).

## 1. Introduction

As a colorless, pungent, and toxic volatile organic compound (VOC), benzene (C<sub>6</sub>H<sub>6</sub>) is seriously detrimental to human health [1–3]. Long-term exposure to even low concentrations (ppb-level) of benzene can cause grievous diseases such as leukemia and lymphomas, and it has also been recognized as a carcinogen by the International Agency for Research on Cancer (IARC) [4]. Therefore, the effective detection of trace benzene seems to be crucially important for the protection of human health. Metal-Oxide-Semiconductor (MOS) gas sensors have been widely used in the detection of benzene because of their low cost and excellent performance [5–8]. Ruan et al. prepared a gas sensor based on rose-shaped ZnO with Au noble metal-modified gas-sensitive material, which exhibited improved gas-sensitive performance toward BTX (benzene, toluene, and xylene) operating at 200 °C [9]. The sensor based on the Co<sub>3</sub>O<sub>4</sub> hierarchical porous structure prepared by Cao et al. showed favorable response/recovery performance against 50 ppm benzene at 220 °C operating temperature, as well as good repeatability and stability [10]. However, conventional MOS-type gas sensors usually operate at high temperatures between 100 °C and 450 °C to obtain improved sensing performance to meet the demand of the reaction activation energy, which leads to high power consumption, reduced life of the sensor, and an increase in the overall cost of the gas sensor, limiting its further practical application.

In recent years, Transition Metal Dichalcogenides (TMDs) offer high surface area and high electron mobility due to their unique 2D structure, making them promising candidates for realization of resistive gas sensors at room temperature [11–15]. For instance, Parne et al. prepared a highly selective and sensitive MoS<sub>2</sub>-based resistance-type gas sensor. The gas sensors of MoS<sub>2</sub> and MoS<sub>2</sub>-based nanocomposites (MoS<sub>2</sub>, MoS<sub>2</sub>-Fe<sub>3</sub>O<sub>4</sub>, and MoS<sub>2</sub>-GO) showed good sensing performance for toluene, which can be attributed to the nanocomposites improving the surface roughness of MoS<sub>2</sub> [16]. Stanciu et al. used a facile solution mixing method to fabricate flexible gas sensors based on Au-functionalized MoS<sub>2</sub> nanoflakes. The results showed that Au/MoS<sub>2</sub> sensors showed excellent sensing performance in terms of sensitivity, selectivity for oxygen-based VOCs, repeatability, and durability at room temperature [17]. Although the use of TMDs as a sensitive material can achieve effective detection at low temperatures, even room temperature, the change of electrical signal caused by the adsorption reaction of trace gas molecules is very weak. Therefore, the resistance gas sensor still faces the problem of difficulty in detecting trace gas effectively. In addition, the gas-sensitive characteristics in the trace gas environment are easily affected by noise signals, which makes it hard for the sensor to capture gas molecules. Therefore, improving the detection and recognition ability of gas sensors for trace gas molecules is the key to achieving the detection of benzene at room temperature.

Recently, with the rapid development of semiconductor technology, a field effect transistor (FET)-type gas sensor has shown great potential because of its high sensitivity, integration, and miniaturization [18–20]. The FET regulates the carrier concentration in the channel through the change of the gate electrical signal. The weak electrical signal change caused by trace gases can be captured and then effectively amplified by the FET-type gas sensor [21,22]. Channel material is one of the important factors affecting the electrical performance of FET. Carbon nanotubes (CNTs), as a typical one-dimensional nanomaterial, are regarded as a potential channel material with advantages such as high electron mobility, extremely small size, and excellent mechanical and electrical properties [23–25]. Zhang et al. optimized the structure of the FET gas sensor by introducing a Y<sub>2</sub>O<sub>3</sub> thin film as the gate insulation layer, which improved various gas-sensitive properties of the sensor; the detection limit of H<sub>2</sub> gas concentration could reach 5 ppb [26], which is expected to replace the traditional resistance-type gas sensor in the field of trace gas detection. Accordingly, it can be predicted that efficient detection of trace benzene at room temperature would be achieved through the combination of TMD-sensitive materials and carbon-based FETs with an amplification effect. In addition, it remains challenging to effectively solve the cross-sensitivity problem for gas sensors toward benzene and its homologs. Typically, the selectivity of gas sensors can be improved by modifying sensing materials and highly porous nanostructures, as well as increasing the operating temperature or adding an external light source [27,28]. However, the above method will lead to shortages, such as changes in material properties, increased power consumption, and sensor costs. Noticeably, Tenax TA, a porous polymer 2,6-diphenyl furan resin, is widely used in the adsorption of VOCs and SVOCs because of its ability to separate molecules by molecular weight and chemical functional groups [29]. Thus, the integration of Tenax TA into gas-sensing devices as the screening unit is expected to solve the cross-sensitivity problem between benzene and its homologs.

Inspired by the above investigations, a CNTs-based FET-type gas sensor based on ZnO/WS<sub>2</sub> nanocomposites has been fabricated for the efficient detection of benzene at room temperature. The ZnO/WS<sub>2</sub> nanocomposites serve as the gate material for the capture of gas molecules, and the CNTs are used as the channel material for electron transfer. The gas-sensitive performance of the as-proposed FET-type gas sensor is investigated in detail. As expected, the CNTs-FET-type gas sensor based on ZnO/WS<sub>2</sub> nanocomposites exhibits high sensitivity toward trace benzene at room temperature and shows desirable stability and repeatability. The Tenax TA screening unit is further used to screen benzene and toluene, which improves the selectivity of the sensor. It is expected that this method can

provide a useful reference for the preparation of integrated, low-power consumption, and portable gas sensors.

## 2. Materials and Methods

### 2.1. Fabrication of FET Gas Sensors

The as-proposed FET-type gas sensor is fabricated onto a carbon-based wafer via the micro–nano manufacturing technologies as depicted in Figure 1a; the commercial carbon-based wafer (4-inch, Peking University) used here is formed from high-purity CNTs randomly distributed on the Si/SiO<sub>2</sub> substrate [30]. The wafer was cut to 11 mm × 11 mm size, and the surface was cleaned for subsequent preparation. Firstly, the pre-defined source (S) and drain (D) electrode regions are lithographed by a laser direct writing lithography machine (Microwriter ML<sup>®</sup>3, Durham Magneto Optics, Ltd., Cambridge, UK). Subsequently, Ti/Pd/Au (0.3/20/40 nm) films are deposited as electrodes by electron beam evaporation (DE400DHL, Beijing Deyi Tianli Technology Development Co. Ltd., Beijing, China) at the rates of 0.1, 1, and 1 Å s<sup>-1</sup>, respectively. In order to prevent mutual interference between different sensors on the same unit, the excess CNTs are etched away by a reactive ion etching machine (Haasrode-R200A, Jiangsu Leuven Instruments Co., Ltd., Peizhou, China) in an oxygen environment of 60 s that would form a conductive channel with a length of 300 nm and a width of 600 nm. Secondly, yttrium (Y) film with a thickness of 3 nm is deposited on the S/D electrode and conductive channel at a rate of 0.1 Å s<sup>-1</sup> by electron beam evaporation and then oxidized at 270 °C for 30 min. By repeating the previous step one more time, yttrium oxide (Y<sub>2</sub>O<sub>3</sub>) film with a thickness of about 10 nm is formed as the gate insulation layer of the FET. The gate insulation layer is usually composed of Y<sub>2</sub>O<sub>3</sub>, Al<sub>2</sub>O<sub>3</sub>, Ta<sub>2</sub>O<sub>5</sub>, Pr<sub>2</sub>O<sub>3</sub>, HfO<sub>2</sub>, and HfSiO<sub>x</sub>. Among them, Y<sub>2</sub>O<sub>3</sub> is an ideal high-κ gate material (dielectric constant of 12–20 and a wide energy gap of 5.5 eV), and the wettability between Y<sub>2</sub>O<sub>3</sub> and CNTs is excellent, so Y<sub>2</sub>O<sub>3</sub> is selected as the gate insulation layer [31]. In addition, Y<sub>2</sub>O<sub>3</sub> can grow uniformly on the surface of the CNTs without degrading key metrics such as gate capacitance and drain current of the FET. The ultrathin Y<sub>2</sub>O<sub>3</sub> film with a high dielectric constant can optimize the sensitivity, selectivity, and stability of the thin film gas sensor through synergistic amplification and protection effects. Therefore, these properties make Y<sub>2</sub>O<sub>3</sub> one of the most promising gate dielectric layers for applications in FET sensors. Finally, the as-prepared ZnO/WS<sub>2</sub> nanocomposites are coated on the FET by drip coating. The package diagram of the FET gas sensor and its optical micrograph can be seen in Figure 1a, where the ZnO/WS<sub>2</sub> layer serves as the floating gate, and the back of the Si substrate acts as the control gate. Details of the preparation of ZnO/WS<sub>2</sub> nanocomposites can be found in the supporting information. The FET gas sensor prepared using the above method is perfectly compatible with semiconductor processing technology, suitable for large-scale sensor production, and ensures good consistency.

### 2.2. Characterization

Raman spectroscopy (Renishaw in Via, Renishaw, Ltd., Wotton-under-Edge, UK) is used to verify the defect degree and conductivity of the CNTs channel. The morphology of CNT films and gas-sensitive materials is investigated by field emission scanning electron microscopy (FE-SEM, Hitachi SU5000, Hitachi, Ltd., Tokyo, Japan). The chemical composition of the materials is characterized by energy-dispersive X-ray spectroscopy (EDS). The composition and chemical state of the gas-sensitive materials are analyzed by X-ray diffraction (XRD, U1tima IV) and X-ray photoelectron spectroscopy (XPS, Thermo ESCALAB 250Xi, Thermo Fisher Scientific, Inc., Waltham, MA, USA).

### 2.3. Gas-Sensing Measurement

The gas-sensing performances of the as-prepared FET-type gas sensor are investigated by the CGS-MT intelligent gas sensitive analysis system, DGL-III Humidity Control gas–liquid distribution system, and the SA3102 electrical analysis system (Beijing Elite Tech Co., Ltd., Beijing, China), as shown in Figure 1b. The electrical performances of CNTs-

based FET are measured by using a Keithly 4200 semiconductor analyzer (Tektronix, Inc., Beaverton, OR, USA) and probe stand (Cascade Microtech MPS 150, Cascade Microtech, Inc., Beaverton, OR, USA). The gas-sensing data are obtained by detecting the current change of the sensor at room temperature (25 °C) with a fixed bias voltage ( $V_{ds} = -0.1$  V). Considering that the bias ( $V_{ds}$ ) has little effect on the gas-sensing response, a small fixed operating voltage (i.e.,  $V_{ds} = -0.1$  V) is chosen in order to prevent device breakdown [32,33]. The dry air (79% N<sub>2</sub> and 21% O<sub>2</sub>) and benzene (100 ppm) are controlled by the combination of the Gas Mass Flow Controller (MFC) of the DGL-III (MFC1 (service range: 20–1000 sccm) and MFC2 (service range: 2–100 sccm)), which is proportionally diluted into different concentrations of benzene, and the total gas flow is fixed at 1000 sccm. It is worth noting that when the gas flow is too low, the gas may be adsorbed by the tube before reaching the sensor, especially at low concentrations. When the gas flow is too high, the sensor signal size and even stability will be affected. From the experience of previous experiments, a fixed flow rate of 1000 sccm ensures that a sufficient amount of the target gas can participate in the reaction without damaging the sensor [34,35]. The testing gases were all purchased from Dalian Special Gas Co., Ltd. (Dalian, China). Gas flow and humidity were controlled using mass flow controllers in DGL-III, and different concentrations of benzene were prepared by the dynamic configuration of the gas distribution system, with the preparation process of interfering gases (such as Toluene, SO<sub>2</sub>, H<sub>2</sub>S, etc.) being like that of the target gas. Before starting the test, dry air is pre-injected into the chamber for 30 min to eliminate the effects of other interfering gases. The response of the FET-type gas sensor can be defined as  $|I_g - I_a| / I_a \times 100\%$ , where  $I_g$  and  $I_a$  are the currents of the sensor in target gas and air, respectively. In order to improve the efficiency of the test, this work uses a fixed time to measure the change in the response of the sensor, that is, 90 s of injection of the target gas. The response/recovery time is expressed as the time required for the current change to reach 90% of the total change. Based on the above-mentioned condition, each test was repeated three times, and each datum was a statistical average unless otherwise mentioned. Relevant parameters are extracted and analyzed using batch processing and statistical functions in Origin software (OriginPro 2021, 9.8.0.200).

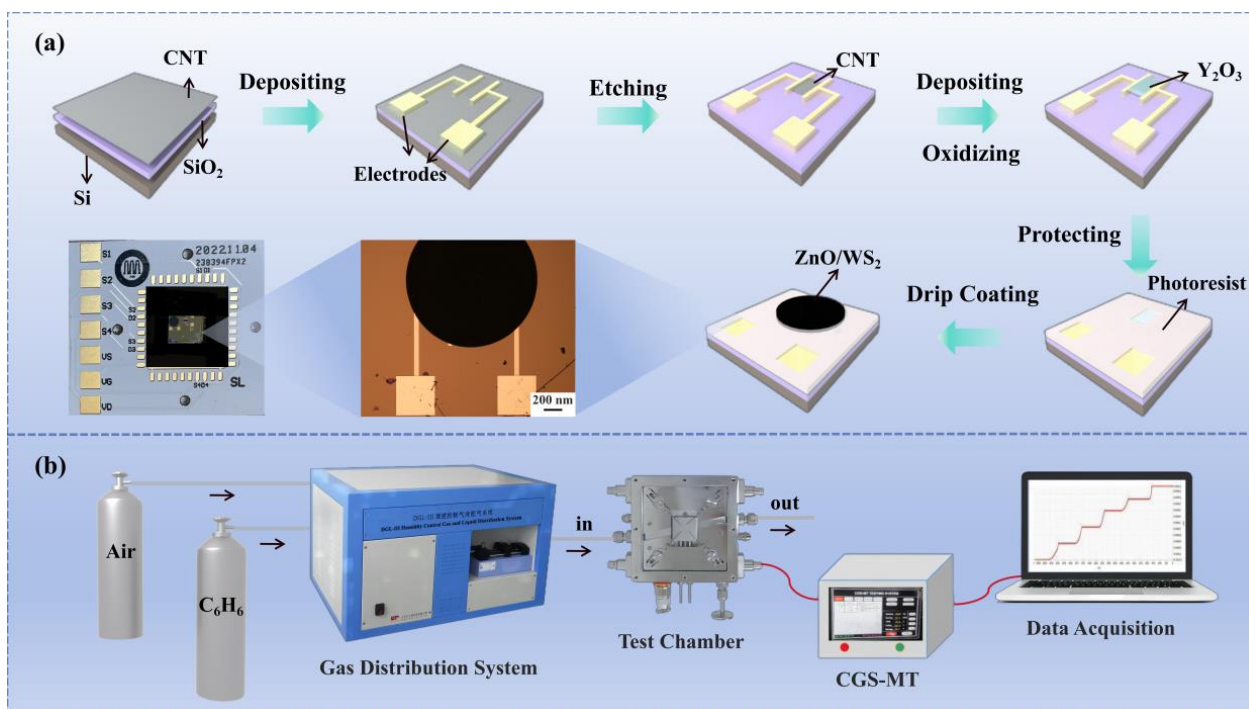


**Figure 1.** (a) Process flow chart of CNTs-based FET gas sensors. (b) Flow chart of gas sensing measurement.

### 3. Results and Discussion

#### 3.1. Characterization Results

For the CNTs-based FET gas sensor, CNTs serve as the channel material to participate in the charge transfer process, and ZnO/WS<sub>2</sub> nanocomposites act as the gate-sensitive material to capture the target gas molecules [36,37]. The low-defect CNT film and the ZnO/WS<sub>2</sub> gas-sensitive material without excess impurities are the keys to achieving the excellent sensing performance of the gas sensor. Therefore, the CNT film is characterized to verify the purity via the Raman spectrum test, as depicted in Figure 2a. It can be observed that the peaks of the RBM peak, D peak, and G peak are located at 170 cm<sup>-1</sup>, 1340 cm<sup>-1</sup>, and 1590 cm<sup>-1</sup>, respectively, which are consistent with the typical Raman characteristic peaks of CNTs [38]. The  $I_G/I_D$  ratio is about 27, and a high  $I_G/I_D$  indicates that CNTs have a high degree of graphitization, less number of defects, and high conductivity [39–42], which provide the foundation for the excellent gas-sensing performance in the subsequent CNTs-based gas sensors. The diameter of CNTs is about 1.45 nm according to the formula  $d$  (nm) = 248/ω (cm<sup>-1</sup>), where ω is the displacement of the RBM peak, and the thin channel can be greatly beneficial to the electrical performance of the gas sensor [33,43]. Figure 2b shows the FE-SEM image of the CNT film, which is distributed in a uniform random grid in the channel region. As described in Figure 2c, it can be clearly observed that a clear and neat boundary is generated between the etched region and the channel region, and there are no CNTs distributed in the etched region, indicating that excess CNTs are etched clean and will not interfere with the electrical properties of the sensor. Then, the morphology and composition of ZnO/WS<sub>2</sub> gas-sensitive materials are analyzed. XRD patterns of ZnO/WS<sub>2</sub> nanocomposites are shown in Figure 2d. It can be seen that the diffraction peaks of ZnO/WS<sub>2</sub> correspond to standard cards (PDF #84-1398) and (PDF #36-1451), respectively, and no impurity diffraction peaks are observed; this proves the high purity of ZnO/WS<sub>2</sub> gas-sensitive material. From the FE-SEM images of ZnO/WS<sub>2</sub>, as illustrated in Figure 2e, ZnO reveals a common spherical structure with a diameter of about 400 nm, and WS<sub>2</sub> presents a flower-like structure consisting of curved thin slices. The flower-like WS<sub>2</sub> can increase the specific surface area and adsorption site and promote the adsorption and penetration of electrons on the material and thus would be conducive to improving the gas-sensitive properties. That is one of the keys for ZnO/WS<sub>2</sub> gas-sensitive materials to realize benzene gas sensing at room temperature. Figure 2f shows the EDS element mapping of ZnO/WS<sub>2</sub> gas-sensitive materials. It can be found that O, S, Zn, and W elements are evenly distributed on the surface, which can prove that the materials are randomly mixed. The full spectrogram is shown in Figure S1; corresponding peaks of Zn 2p, O 1s (adsorbent oxygen and lattice oxygen), S 2p, and W 4f further prove that ZnO/WS<sub>2</sub> gas-sensitive materials have been successfully prepared.

#### 3.2. Gas-Sensing Performance

The premise of a high-performance FET gas sensor is to have excellent electrical performance, and then the transfer characteristic curves of 30 FET sensors in three-chip units (the range of Gate Voltage ( $V_{gs}$ ) is from -60 V to +40 V) are tested, as shown in Figure 3a. It can be seen that all transfer characteristic curves of FETs reveal relatively high consistency with p-type characteristics, and the switching ratio can reach up to four orders of magnitude, which makes the FETs possess very reliable electrical performance [44]. The transfer characteristic curve of the FET gas sensor is shown in Figure 3b. It can be seen that the FET gas sensor exhibits the characteristics of depletion type FET, which is in the “on-on” state when the gate voltage ( $V_{gs}$ ) is set as 0 V [45]. Compared with FET, the transfer characteristic curve of the sensor is positively offset, which can be attributed to the change of electron transport between WS<sub>2</sub> and ZnO and the carrier concentration in the channel [46,47].

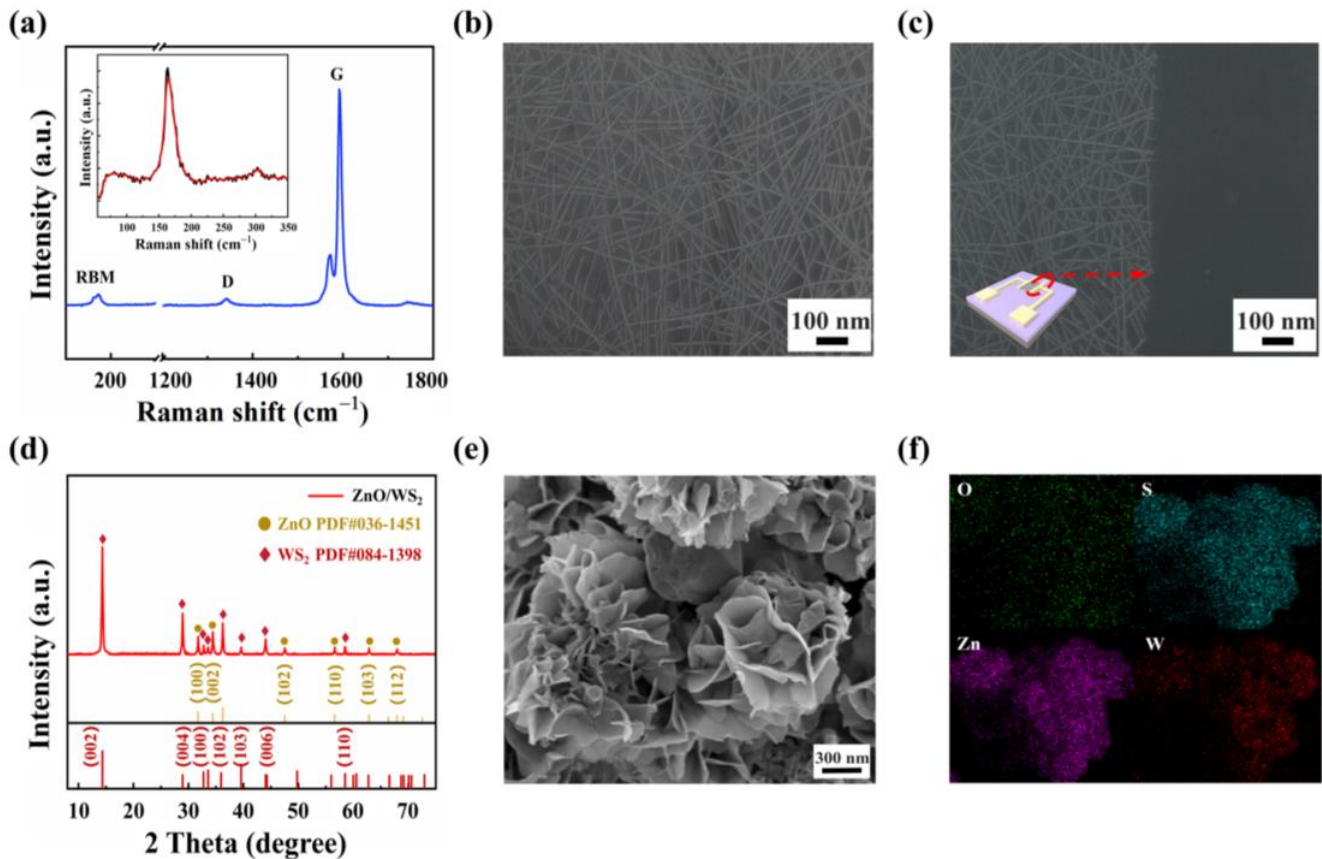


**Figure 2.** (a) Raman characterization of CNT film. FE-SEM image of the (b) CNT film and (c) CNTs region after etching. (d) XRD patterns of ZnO/WS<sub>2</sub>. (e) FE-SEM image of the ZnO/WS<sub>2</sub>. (f) EDS elemental mappings of O, S, Zn, and W.

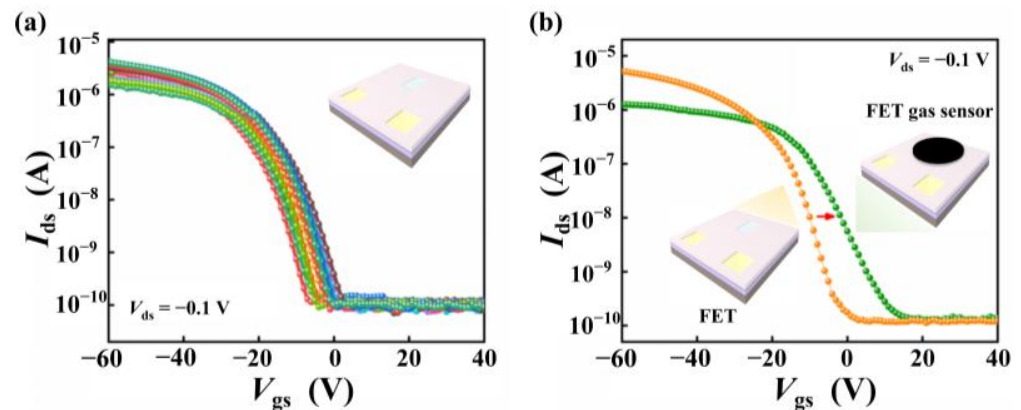


**Figure 3.** (a) Transfer characteristic curves of the FET sensors. (b) The transfer characteristic curves of the FET and FET gas sensor with bias voltage ( $V_{ds} = -0.1$  V).

The gate voltage is an important parameter affecting the gas-sensing performance of the FET-type gas sensor. In order to obtain the best working gate voltage, the response of the FET gas sensor to 1 ppm benzene at different  $V_{gs}$  is measured first, as depicted in Figure S2. When  $V_{gs}$  increases from  $-5$  V to  $5$  V, the response shows no obvious change trend. Taking into account the power consumption of the sensor, the  $V_{gs}$  is set to  $0$  V. Figure S3 shows the response/recovery curve of the FET gas sensor tested under 1 ppm benzene. It can be found that the response time of the sensor is  $90$  s, which has a fast response rate, but the recovery time is relatively slow. Considering that the recovery performance of the sensor is not strictly required in the actual application scenarios in industrial sites, just the

fast response speed can meet the detection needs, the recovery characteristic of the sensor is no longer considered in the subsequent experiments, and only the response characteristic is evaluated as a performance indicator. As shown in Figure S4, the response curve of a FET under 1 ppm benzene is tested; the curve shows that the FET has no response to benzene, which proves that the response of the sensor to benzene is attributable to the ZnO/WS<sub>2</sub> nanocomposites. In order to evaluate the response characteristics of the sensor to benzene in the allowable concentration range, dynamic response curves of the FET gas sensor at the range of 0.5–2 ppm C<sub>6</sub>H<sub>6</sub> are shown in Figure 4a. The  $|I_{ds}|$  of the sensor increases when exposed to benzene and decreases when switched back to air. As the concentration increases, the sensor's  $|I_{ds}|$  also increases. The response fitting curve is shown in Figure 4b. The response of the sensor has an excellent linear distribution with the increase of gas concentration. The sensor can detect benzene as low as 500 ppb and has a lower theoretical detection limit [48]. In this work, a resistance-type gas sensor based on ZnO/WS<sub>2</sub> nanocomposites is also prepared, as shown in Figure S5. The concentration range of 0.5–2 ppm benzene is measured on the ZnO/WS<sub>2</sub>-based resistance-type gas sensor, as shown in Figure S6. It can be found that this sensor has no obvious response when exposed to ppb-level benzene, just a slight change at 1 ppm. By comparison, it can be concluded that the amplification effect of FET can further reduce the detection limit, resulting in the FET gas sensor manifesting a higher sensitivity. According to the standards issued by the European Union for the allowable concentration of gas in industrial sites, the allowable concentration of benzene is set at 0.5 ppm and 1 ppm according to the actual situation [49]. Therefore, dynamic response curves of the sensor at 0.5 ppm and 1 ppm C<sub>6</sub>H<sub>6</sub> for three cycles are further recorded, as depicted in Figure 4c. During a fixed response time (90 s), the sensor reveals the same response characteristic in each cycle; the current changes are almost the same, and it has stable response values of 0.5% and 1.9% in 0.5 ppm and 1 ppm benzene, respectively. Upon exposure to 1 ppm benzene, the current baseline of the sensor is shifted upward, which may be due to the incomplete recovery of the sensor due to the long recovery time (>3600 s). When sufficient air is injected, the sensor's current baseline can be restored to the initial level without affecting subsequent detection. In addition, the multi-lot repeatability of the sensor is evaluated. As shown in Figure 4d, it can be seen that a total of nine sensors in three units show excellent response consistency with a response error of less than 5% at 0.5 ppm, 1.0 ppm, and 1.5 ppm benzene, respectively, which confirmed that the prepared devices possess satisfactory reproducibility. The sensor was stored in ambient air without power and was discontinuously tested multiple times for 28 days, with each exposure being to 0.5 ppm, 1.0 ppm, and 1.5 ppm benzene for 4.5 min (three cycles), as shown in Figure 4e. The response error of the sensor is less than 10%, showing ideal stability. Notably, the gas sensor is usually susceptible to interference from water molecules, especially when working at room temperature [50]. Therefore, moisture resistance should also serve as a common index to evaluate the performance of gas-sensing devices. The response curve of the sensor to 1 ppm benzene at 0.4–70% relative humidity (RH) is then evaluated, as shown in Figure S7. It can be seen that with the increase of RH, the response value of the sensor gradually decreases, which means that the moisture resistance of the sensor is general, mainly due to the competition between water molecules and benzene molecules. Since the sensor has a certain cross-response phenomenon to the interference gas, selectivity needs to be fully considered as an important influence parameter of the sensor [51]. As shown in Figure 4f, the gas-sensing characteristics of the FET gas sensor are measured toward different common polluting gases (i.e., SO<sub>2</sub>, H<sub>2</sub>S, CH<sub>3</sub>OH, HCHO, NH<sub>3</sub>, C<sub>3</sub>H<sub>6</sub>O, and C<sub>7</sub>H<sub>8</sub>) in industrial sites at a concentration of 1 ppm. It can be found that the response of the sensor to these gases, except toluene, is very low, less than half of benzene. The similar response toward benzene and toluene is due to the fact that they belong to a homolog and have similar molecular functional groups.

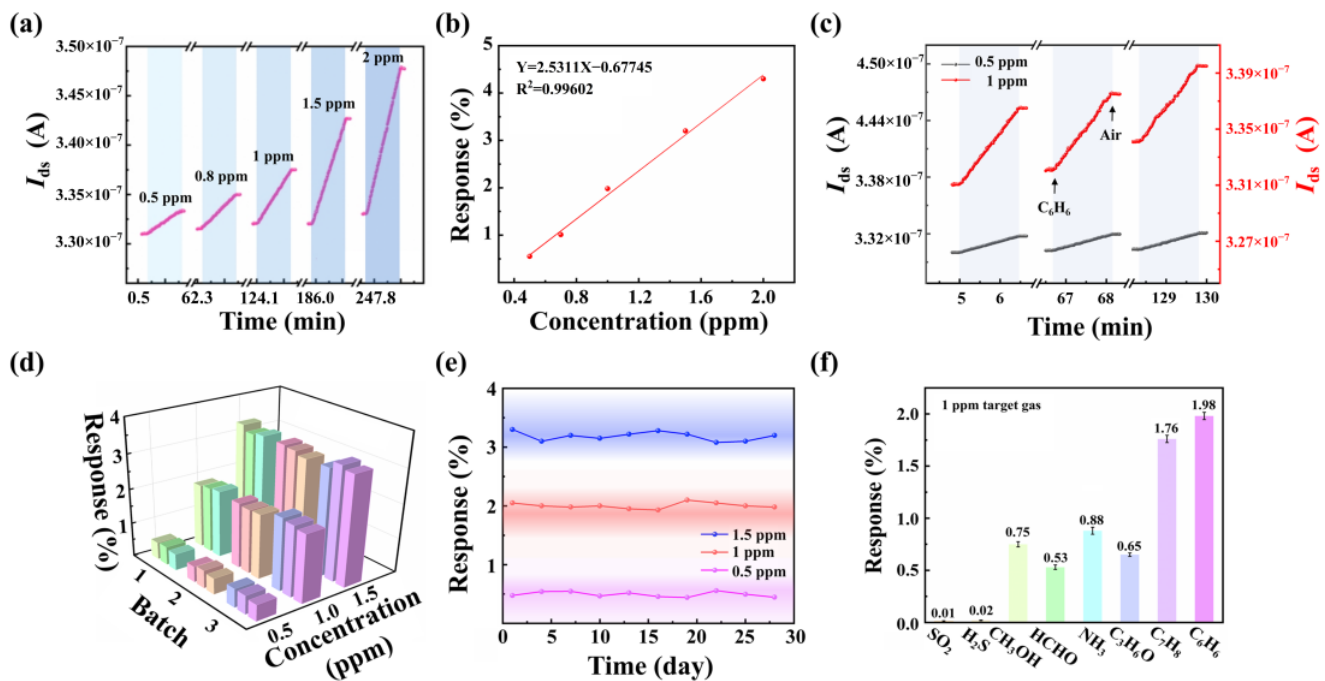


**Figure 4.** (a) Dynamic response curves of the FET gas sensor at the range of 0.5–2 ppm  $C_6H_6$ . (b) The response fitting curve. (c) Dynamic response curves of the FET gas sensor at 0.5 ppm and 1 ppm  $C_6H_6$  for three cycles, respectively. (d) Response values for a total of 9 FET gas sensors selected from 3 batches. (e) The response values of the FET gas sensor measured several times within 28 days. (f) The response values of the FET gas sensor toward different gases at 1 ppm.

In order to solve the problem of cross-sensitivity between benzene and toluene, the Tenax TA screening unit has been prepared for this work. Owing to its unique physical structure, Tenax TA particles can effectively separate benzene and toluene based on the difference in the adsorption time of gas molecules [29]. The schematic diagram of the structure of the sensor is shown in Figure S8a. The Tenax TA screening unit is composed of a hard Teflon tube with an inner diameter of 4 mm and a length of 90 mm, which is filled with 150 mg Tenax TA particles. The internal package structure diagram of the FET gas sensor is shown in Figure S8b. The FET gas sensor is fixed on the metallic substrate. The FE-SEM image of the Tenax TA particle is shown in Figure S8c. It can be observed that the Tenax TA particle presents a highly porous structure, which is the key to its ability to achieve gas adsorption and separation. To verify the successful separation effect of the Tenax TA screening unit, the gas-sensitive performance of the gas sensor with the Tenax TA screening unit is tested. The response curves of the FET gas sensor to 2 ppm benzene and 2 ppm toluene with or without the Tenax TA screening unit are first tested, as shown in Figures 5a and 5b, respectively. Through comparison, it can be obviously observed that there is a delay in the response curve; the retention time is 5.2 min and 16.3 min, respectively, which is basically consistent with the gas retention time of benzene and toluene in the previous report [29]. Notably, the response value of the gases is attenuated, which is due to the insufficient elution of benzene and toluene gases by the Tenax TA screening unit. Figure 5c shows the response curve of the FET gas sensor toward mixed gas, including 2 ppm benzene and 2 ppm toluene. It can be found that two peaks appear at different times: the first peak at 5.3 min is the peak corresponding to benzene, and the second peak at 16.4 min is the peak corresponding to toluene. Benzene can be successfully screened from the mixed gas and effectively detected. Therefore, the Tenax TA screening unit successfully realizes the separation of benzene and toluene, which improves the selectivity of the FET gas sensor.

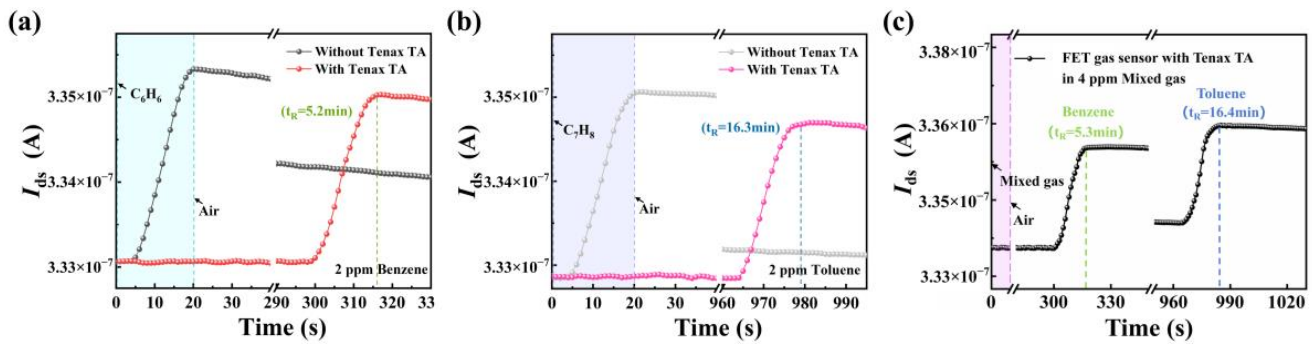
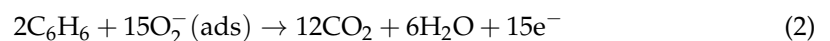


**Figure 5.** The response curves of the FET gas sensor to (a) 2 ppm benzene and (b) 2 ppm toluene with or without the Tenax TA screening unit. (c) The mixed gas test diagram of the FET gas sensor with the Tenax TA screening unit.

### 3.3. Gas-Sensing Mechanism

The gas-sensing mechanism of the FET gas sensor can be explained theoretically by Figure 6. As shown in Figure 6a, ZnO work function is smaller than WS<sub>2</sub>, resulting in electron flow from ZnO to WS<sub>2</sub>. When the gas sensor is exposed to oxygen, O<sub>2</sub> molecules will obtain electrons from ZnO. Meanwhile, electrons transferred from ZnO to WS<sub>2</sub> will also be captured by O<sub>2</sub> molecules, and then the Fermi level will bend until equilibrium is balanced [52]. O<sub>2</sub> molecules are adsorbed on the surface of the ZnO/WS<sub>2</sub> nanocomposites in the form of adsorbed oxygen ions (O<sub>2</sub><sup>−</sup>(ads)) to form an electron aggregation layer, and then the holes in the channel will transfer to the gate dielectric layer interface via the dipole–dipole interaction [33]. Therefore, the hole concentration in the channel will be reduced, which can lead to the reduction of  $|I_{ds}|$ . As shown in Figure 6b, when the gas sensor is exposed to benzene, the reducing benzene molecules react with O<sub>2</sub><sup>−</sup>(ads), releasing the captured electrons back into ZnO, and the Fermi level changes again. The decrease of electrons on the surface of the material will cause the holes at the gate dielectric layer interface to be released back into the channel, the hole concentration in the channel will increase, and the  $|I_{ds}|$  of the FET gas sensor will increase, which is consistent with the response of the gas sensor to benzene in the above experiments. The equations for the reaction of the gas sensor exposed to air and benzene are as follows:



The remarkable gas-sensing performance of the sensor can be attributed to the structure of the FET sensor and the use of ZnO/WS<sub>2</sub> nanocomposites. Based on the working principle of FET, the gate-sensitive material produces a chemical signal after contact with the target gas molecules; the chemical signal will be converted into a gate electrical signal. The unique gate control characteristics of FET can be used to adjust the current between the source and drain to achieve the amplification of the weak gas-sensing signal [53–55]. CNTs, as the channel material of FET, have extremely high carrier mobility, and they can provide a high-speed channel for carrier transmission. A small change in the gate electrical signal can cause a large change in the conductivity of the FET [56,57]. Y<sub>2</sub>O<sub>3</sub> is regarded as an ideal material for the gate dielectric layer due to its good interface with CNTs and high  $\kappa$  value. The isolation between the conductive layer and the gas-sensitive layer avoids interference from external gas molecules in the channel; the gas reaction process only occurs on the gas-sensitive layer, thus improving the reliability and stability of the FET sensor [58,59]. In addition, the flower-like WS<sub>2</sub> provides more adsorption sites, which is conducive to the adsorption and penetration of gas molecules, eventually facilitating the gas-sensing performances of the as-proposed carbon-based FET-type gas sensor. Furthermore, due to the difference in van der Waals forces between the Tenax TA particles and different gas molecules, the adsorption time in the screening unit is different, and they will eluate at

the corresponding time. The introduction of the screening unit successfully realizes the separation of benzene and toluene and improves the selectivity of the sensor.

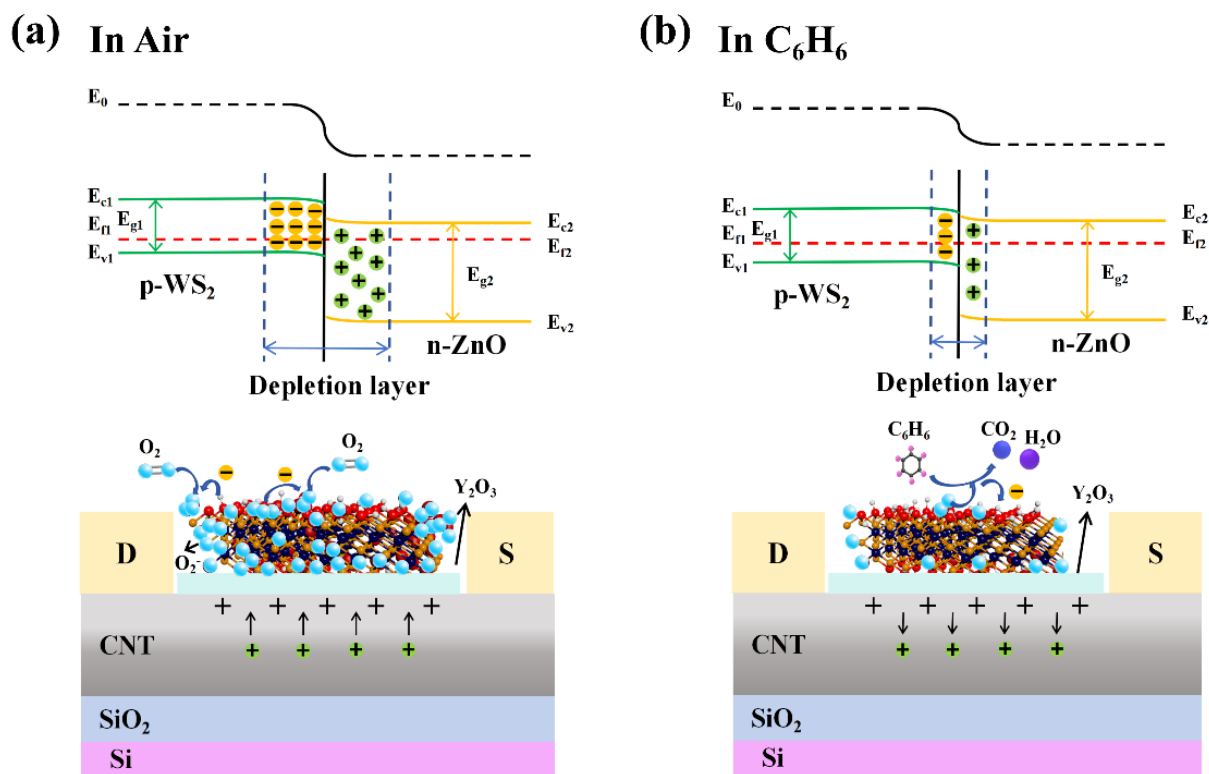


Figure 6. Schematic illustrations of the gas-sensing mechanisms (a) in air and (b) in C<sub>6</sub>H<sub>6</sub>.

#### 4. Conclusions

To sum up, in this work, a carbon-based FET-type gas sensor for the detection of trace benzene at room temperature has been successfully prepared by using micro–nano processing technology. ZnO/WS<sub>2</sub> nanocomposites serve as gate materials to participate in the gas-sensitive response, and CNTs are used as channel materials to be involved in charge transport. The gas-sensing layer and the transfer layer are isolated by the Y<sub>2</sub>O<sub>3</sub> dielectric layer to play their respective roles. Based on the amplification effect of FET, the as-proposed gas sensor reveals a low detection limit to benzene, as low as 500 ppb at room temperature. It also has excellent stability and repeatability, and the response value error of multi-batch sensors is less than 5%. The portable Tenax TA screening unit has been fabricated and then combined with the FET gas sensor to screen benzene from the mixed gas, which can solve the cross-sensitive problem of the sensor to benzene and toluene. The selectivity of the gas sensor can thus be improved by using the portable Tenax TA screening unit. It is expected that this work will provide a reference for the exploitation of high-performance gas sensors for the efficient identification and detection of trace gases in industrial sites and environmental monitoring.

**Supplementary Materials:** The following supporting information can be downloaded at: <https://www.mdpi.com/article/10.3390/chemosensors12090179/s1>, Figure S1: The full spectrogram of ZnO/WS<sub>2</sub> nanocomposites; Figure S2: The response of the FET gas sensor at different V<sub>gs</sub>; Figure S3: The response/recovery curve of the FET gas sensor toward 1 ppm benzene; Figure S4: The response curve of FET toward 1 ppm benzene; Figure S5: The diagram of the resistance-type gas sensor; Figure S6: Dynamic response curves of ZnO/WS<sub>2</sub>-based resistance-type gas sensor at the range of 0.5–2 ppm C<sub>6</sub>H<sub>6</sub>; Figure S7: The response curve of the FET gas sensor at 0.4–70% relative humidity (RH); Figure S8: (a) The schematic diagram of the structure of the sensor. (b) The internal package structure diagram of the FET gas sensor. (c) The FE-SEM image of Tenax TA particles.

**Author Contributions:** Conceptualization, J.H. and Y.Z.; methodology, J.H. and Y.Z.; validation, R.C. and Z.L.; investigation, R.C. and Z.L.; writing—original draft preparation, R.C. and Z.L.; writing—review and editing, R.C., J.H., and Y.Z.; supervision, J.H. and Y.Z.; funding acquisition, J.H. and Y.Z. All authors have read and agreed to the published version of the manuscript.

**Funding:** This research was funded by the National Natural Science Foundation of China (62071410, 62101477, 62471425) and the Science and Technology Innovation Program of Hunan Province (2023RC3133).

**Institutional Review Board Statement:** Not applicable.

**Informed Consent Statement:** Not applicable.

**Data Availability Statement:** Data are available from the authors under reasonable request.

**Conflicts of Interest:** The authors declare no conflicts of interest.

## References

1. Mirzaei, A.; Kim, J.-H.; Kim, H.W.; Kim, S.S. Resistive-based gas sensors for detection of benzene, toluene and xylene (BTX) gases: A review. *J. Mater. Chem. C* **2018**, *6*, 4342–4370. [[CrossRef](#)]
2. Zhang, Y.; Rong, Q.; Zhao, J.; Zhang, J.; Zhu, Z.; Liu, Q. Boron-doped graphene quantum dot/Ag–LaFeO<sub>3</sub> p–p heterojunctions for sensitive and selective benzene detection. *J. Mater. Chem. A* **2018**, *6*, 12647–12653. [[CrossRef](#)]
3. Zhu, M.-Y.; Zhang, L.-X.; Yin, J.; Chen, J.-J.; Bie, L.-J. Ppt-level benzene detection and gas sensing mechanism using (C<sub>4</sub>H<sub>9</sub>NH<sub>3</sub>)<sub>2</sub>PbI<sub>2</sub>Br<sub>2</sub> organic–inorganic layered perovskite. *Inorg. Chem. Front.* **2018**, *5*, 3046–3052. [[CrossRef](#)]
4. Raaschou-Nielsen, O.; Hvidtfeldt, U.A.; Roswall, N.; Hertel, O.; Poulsen, A.H.; Sørensen, M. Ambient benzene at the residence and risk for subtypes of childhood leukemia, lymphoma and CNS tumor. *Int. J. Cancer* **2018**, *143*, 1367–1373. [[CrossRef](#)] [[PubMed](#)]
5. Kim, J.-H.; Mirzaei, A.; Kim, H.W.; Kim, S.S. Pd-functionalized core-shell composite nanowires for self-heating, sensitive, and benzene-selective gas sensors. *Sens. Actuators A* **2020**, *308*, 112011. [[CrossRef](#)]
6. Vaishnav, V.S.; Patel, S.G.; Panchal, J.N. Development of ITO thin film sensor for detection of benzene. *Sens. Actuators B* **2015**, *206*, 381–388. [[CrossRef](#)]
7. Kim, W.-T.; Kim, I.-H.; Choi, W.-Y. Fabrication of TiO<sub>2</sub> Nanotube Arrays and Their Application to a Gas Sensor. *J. Nanosci. Nanotechnol.* **2015**, *15*, 8161–8165. [[CrossRef](#)]
8. Wang, L.; Wang, S.; Xu, M.; Hu, X.; Zhang, H.; Wang, Y.; Huang, W. A Au-functionalized ZnO nanowire gas sensor for detection of benzene and toluene. *Phys. Chem. Chem. Phys.* **2013**, *15*, 17179–17186. [[CrossRef](#)]
9. Shen, Z.; Zhang, X.; Ma, X.; Mi, R.; Chen, Y.; Ruan, S. The significant improvement for BTX (benzene, toluene and xylene) sensing performance based on Au-decorated hierarchical ZnO porous rose-like architectures. *Sens. Actuators B* **2018**, *262*, 86–94. [[CrossRef](#)]
10. Cao, J.; Wang, S.; Li, J.; Xing, Y.; Zhao, X.; Li, D. Porous nanosheets assembled Co<sub>3</sub>O<sub>4</sub> hierarchical architectures for enhanced BTX (Benzene, Toluene and Xylene) gas detection. *Sens. Actuators B* **2020**, *315*, 128120. [[CrossRef](#)]
11. Hu, J.; Zhang, J.; Liu, X.; Zhang, H.; Xue, X.-X.; Zhang, Y. Highly selective NO<sub>2</sub> sensor based on Au/SnS<sub>2</sub> nano-heterostructures via visible-light modulation. *Appl. Surf. Sci.* **2023**, *623*, 157093. [[CrossRef](#)]
12. Hu, J.; Liu, X.; Zhang, J.; Gu, X.; Zhang, Y. Plasmon-activated NO<sub>2</sub> sensor based on Au@MoS<sub>2</sub> core-shell nanoparticles with heightened sensitivity and full recoverability. *Sens. Actuators B* **2023**, *382*, 133505. [[CrossRef](#)]
13. Chen, X.; Hu, J.; Chen, P.; Yin, M.; Meng, F.; Zhang, Y. UV-light-assisted NO<sub>2</sub> gas sensor based on WS<sub>2</sub>/PbS heterostructures with full recoverability and reliable anti-humidity ability. *Sens. Actuators B* **2021**, *339*, 129902. [[CrossRef](#)]
14. Liu, J.-B.; Hu, J.-Y.; Liu, C.; Tan, Y.-M.; Peng, X.; Zhang, Y. Mechanically exfoliated MoS<sub>2</sub> nanosheets decorated with SnS<sub>2</sub> nanoparticles for high-stability gas sensors at room temperature. *Rare Met.* **2020**, *40*, 1536–1544. [[CrossRef](#)]
15. Xin, X.; Zhang, Y.; Guan, X.; Cao, J.; Li, W.; Long, X.; Tan, X. Enhanced Performances of PbS Quantum-Dots-Modified MoS<sub>2</sub> Composite for NO<sub>2</sub> Detection at Room Temperature. *ACS Appl. Mater. Interfaces* **2019**, *11*, 9438–9447. [[CrossRef](#)]
16. Thayil, R.; Krishna, K.G.; Cherukulappurath, S.; Kathirvelu, V.; Parne, S.R. MoS<sub>2</sub> and MoS<sub>2</sub>-based nanocomposites for enhanced toluene sensing response at room temperature. *Surf. Interfaces* **2024**, *46*, 104134. [[CrossRef](#)]
17. Alev, O.; Özdemir, O.; Goldenberg, E.; Çolakeroğlu Arslan, L.; Büyükköse, S.; Öztürk, Z.Z. WS<sub>2</sub> thin film based quartz crystal microbalance gas sensor for dimethyl methylphosphonate detection at room temperature. *Thin Solid Films* **2022**, *745*, 139097. [[CrossRef](#)]
18. Fahad, H.M.; Shiraki, H.; Amani, M.; Zhang, C.; Hebbbar, V.S.; Gao, W.; Ota, H.; Hettick, M.; Kiriya, D.; Chen, Y.-Z.; et al. Room temperature multiplexed gas sensing using chemical-sensitive 3.5-nm-thin silicon transistors. *Sci. Adv.* **2017**, *3*, e1602557. [[CrossRef](#)]
19. Yuan, Z.; Bariya, M.; Fahad, H.M.; Wu, J.; Han, R.; Gupta, N.; Javey, A. Trace-Level, Multi-Gas Detection for Food Quality Assessment Based on Decorated Silicon Transistor Arrays. *Adv. Mater.* **2020**, *32*, e1908385. [[CrossRef](#)]
20. Mukherjee, A.; Rosenwaks, Y. Recent Advances in Silicon FET Devices for Gas and Volatile Organic Compound Sensing. *Chemosensors* **2021**, *9*, 260. [[CrossRef](#)]

21. Hong, S.; Wu, M.; Hong, Y.; Jeong, Y.; Jung, G.; Shin, W.; Park, J.; Kim, D.; Jang, D.; Lee, J.-H. FET-type gas sensors: A review. *Sens. Actuators B* **2021**, *330*, 129240. [[CrossRef](#)]
22. Tang, X.; Raskin, J.-P.; Reckinger, N.; Yan, Y.; André, N.; Lahem, D.; Debliquy, M. Enhanced Gas Detection by Altering Gate Voltage Polarity of Polypyrrole/Graphene Field-Effect Transistor Sensor. *Chemosensors* **2022**, *10*, 467. [[CrossRef](#)]
23. Onyancha, R.B.; Aigbe, U.O.; Ukhurebor, K.E.; Muchiri, P.W. Facile synthesis and applications of carbon nanotubes in heavy-metal remediation and biomedical fields: A comprehensive review. *J. Mol. Struct.* **2021**, *1238*, 130462. [[CrossRef](#)]
24. Kong, J.; Franklin, N.R.; Zhou, C.; Chapline, M.G.; Peng, S.; Cho, K.; Dai, H. Nanotube Molecular Wires as Chemical Sensors. *Science* **2000**, *287*, 622–625. [[CrossRef](#)] [[PubMed](#)]
25. Shooshtari, M.; Salehi, A. An electronic nose based on carbon nanotube-titanium dioxide hybrid nanostructures for detection and discrimination of volatile organic compounds. *Sens. Actuators A* **2022**, *357*, 131418. [[CrossRef](#)]
26. Zhou, S.; Xiao, M.; Liu, F.; He, J.; Lin, Y.; Zhang, Z. Sub-10 parts per billion detection of hydrogen with floating gate transistors built on semiconducting carbon nanotube film. *Carbon* **2021**, *180*, 41–47. [[CrossRef](#)]
27. Wawrzyniak, J. Advancements in Improving Selectivity of Metal Oxide Semiconductor Gas Sensors Opening New Perspectives for Their Application in Food Industry. *Sensors* **2023**, *23*, 9548. [[CrossRef](#)] [[PubMed](#)]
28. Wang, T.; Chen, J.; Chen, J.; Yao, X.; Chen, G.; Jiao, Z.; Zhao, J.-T.; Cheng, S.; Yang, X.-C.; Li, Q. UV-light enhanced gas sensor based on Ga doped ZnO for ultra-high sensitive and selective n-butanol detection. *Appl. Surf. Sci.* **2023**, *641*, 158551. [[CrossRef](#)]
29. van den Broek, J.; Abegg, S.; Pratsinis, S.E.; Güntner, A.T. Highly selective detection of methanol over ethanol by a handheld gas sensor. *Nat. Commun.* **2019**, *10*, 4220. [[CrossRef](#)]
30. Xiao, M.; Liang, S.; Han, J.; Zhong, D.; Liu, J.; Zhang, Z.; Peng, L. Batch Fabrication of Ultrasensitive Carbon Nanotube Hydrogen Sensors with Sub-ppm Detection Limit. *ACS Sens.* **2018**, *3*, 749–756. [[CrossRef](#)]
31. Pan, T.-M.; Chang, C.-J. High-performance poly-silicon TFTs with high- $\kappa$   $Y_2O_3$  gate dielectrics. *Semicond. Sci. Technol.* **2011**, *26*, 075004. [[CrossRef](#)]
32. Dassi, M.; Madan, J.; Pandey, R.; Sharma, R. Magnesium silicide source double palladium metal gate TFET for highly sensitive hydrogen gas sensor. In Proceedings of the 2021 Devices for Integrated Circuit (DevIC) 2021, Kalyani, India, 19–20 May 2021; pp. 238–241. [[CrossRef](#)]
33. Zou, Q.; Liu, B.; Zhang, Y. Design of an array structure for carbon-based field-effect-transistor type gas sensors to accurately identify trace gas species. *J. Mater. Chem. A* **2023**, *11*, 15811–15820. [[CrossRef](#)]
34. Shi, L.; Tang, P.; Hu, J.; Zhang, Y. A Strategy for Multigas Identification Using Multielectrical Parameters Extracted from a Single Carbon-Based Field-Effect Transistor ACS Sens. **2024**, *9*, 3126–3136. 9. [[CrossRef](#)]
35. Tao, L.; Tang, P.; Hu, J.; Zhang, Y. The alcohol lock built on carbon-based field-effect transistor sensor with Pd/ZnO floating gate structure used for drunk driving surveillance. *Sens. Actuators B* **2024**, *419*, 136393. [[CrossRef](#)]
36. Liu, C.; Hu, J.; Wu, G.; Cao, J.; Zhang, Z.; Zhang, Y. Carbon Nanotube-Based Field-Effect Transistor-Type Sensor with a Sensing Gate for Ppb-Level Formaldehyde Detection. *ACS Appl. Mater. Interfaces* **2021**, *13*, 56309–56319. [[CrossRef](#)] [[PubMed](#)]
37. Star, A.; Han, T.R.; Joshi, V.; Gabriel, J.C.P.; Grüner, G. Nanoelectronic Carbon Dioxide Sensors. *Adv. Mater.* **2004**, *16*, 2049–2052. [[CrossRef](#)]
38. Kalbac, M.; Hsieh, Y.-P.; Farhat, H.; Kavan, L.; Hofmann, M.; Kong, J.; Dresselhaus, M.S. Defects in Individual Semiconducting Single Wall Carbon Nanotubes: Raman Spectroscopic and in Situ Raman Spectroelectrochemical Study. *Nano Lett.* **2010**, *10*, 4619–4626. [[CrossRef](#)]
39. Ma, Y.; Ma, J.; Lv, Y.; Liao, J.; Ji, Y.; Bai, H. Effect of mono vacancy defect on the charge carrier mobility of carbon nanotubes: A case study on (10, 0) tube from first-principles. *Superlattices Microstruct.* **2016**, *99*, 140–144. [[CrossRef](#)]
40. Wang, G. Density functional study on the increment of carrier mobility in armchair graphene nanoribbons induced by Stone–Wales defects. *Phys. Chem. Chem. Phys.* **2011**, *13*, 11939–11945. [[CrossRef](#)] [[PubMed](#)]
41. Lucchese, M.M.; Stavale, F.; Ferreira, E.H.M.; Vilani, C.; Moutinho, M.V.O.; Capaz, R.B.; Achete, C.A.; Jorio, A. Quantifying ion-induced defects and Raman relaxation length in graphene. *Carbon* **2010**, *48*, 1592–1597. [[CrossRef](#)]
42. Destyorini, F.; Irmawati, Y.; Hardiansyah, A.; Prato, M.; Widodo, H.; Yahya, I.; Indayaningsih, N.; Yudianti, R.; Hsu, Y.-I.; Uyama, H. Formation of nanostructured graphitic carbon from coconut waste via low-temperature catalytic graphitization. *Eng. Sci. Technol. Int. J.* **2021**, *24*, 514–523. [[CrossRef](#)]
43. Kumar, R.; Aykol, M.; Cronin, S.B. Effect of nanotube-nanotube coupling on the radial breathing mode of carbon nanotubes. *Phys. Rev. B* **2008**, *78*, 165428. [[CrossRef](#)]
44. Li, Z.; Jinkins, K.R.; Cui, D.; Chen, M.; Zhao, Z.; Arnold, M.S.; Zhou, C. Air-stable n-type transistors based on assembled aligned carbon nanotube arrays and their application in complementary metal-oxide-semiconductor electronics. *Nano Res.* **2021**, *15*, 864–871. [[CrossRef](#)]
45. Luo, M.; Zhu, M.; Wei, M.; Shao, S.; Robin, M.; Wei, C.; Cui, Z.; Zhao, J.; Zhang, Z. Radiation-Hard and Repairable Complementary Metal–Oxide–Semiconductor Circuits Integrating n-type Indium Oxide and p-type Carbon Nanotube Field-Effect Transistors. *ACS Appl. Mater. Interfaces* **2020**, *12*, 49963–49970. [[CrossRef](#)]
46. Wang, B.; Li, H.; Tan, H.; Gu, Y.; Chen, L.; Ji, L.; Sun, Z.; Sun, Q.; Ding, S.; Zhang, D.W.; et al. Gate-Modulated High-Response Field-Effect Transistor-Type Gas Sensor Based on the  $MoS_2$ /Metal–Organic Framework Heterostructure. *ACS Appl. Mater. Interfaces* **2022**, *14*, 42356–42364. [[CrossRef](#)]

47. Khalil, H.M.W.; Khan, M.F.; Eom, J.; Noh, H. Highly Stable and Tunable Chemical Doping of Multilayer WS<sub>2</sub> Field Effect Transistor: Reduction in Contact Resistance. *ACS Appl. Mater. Interfaces* **2015**, *7*, 23589–23596. [[CrossRef](#)]
48. Liu, J.; Hu, Z.; Zhang, Y.; Li, H.-Y.; Gao, N.; Tian, Z.; Zhou, L.; Zhang, B.; Tang, J.; Zhang, J.; et al. MoS<sub>2</sub> Nanosheets Sensitized with Quantum Dots for Room-Temperature Gas Sensors. *Nano Micro Lett.* **2020**, *12*, 24–36. [[CrossRef](#)]
49. Kirkeleit, J.; Riise, T.; Gjertsen, B.T.; Moen, B.E.; Bratveit, M.; Bruslerud, O. Effects of Benzene on Human Hematopoiesis. *Open Hematol. J.* **2008**, *2*, 87–102. [[CrossRef](#)]
50. Hu, J.; Wang, X.; Lei, H.; Luo, M.; Zhang, Y. Plasmonic photothermal driven MXene-based gas sensor for highly sensitive NO<sub>2</sub> detection at room temperature. *Sens. Actuators B* **2024**, *407*, 135422. [[CrossRef](#)]
51. Hong, J.; Lee, S.; Seo, J.; Pyo, S.; Kim, J.; Lee, T. A Highly Sensitive Hydrogen Sensor with Gas Selectivity Using a PMMA Membrane-Coated Pd Nanoparticle/Single-Layer Graphene Hybrid. *ACS Appl. Mater. Interfaces* **2015**, *7*, 3554–3561. [[CrossRef](#)]
52. Zhang, D.; Wu, J.; Li, P.; Cao, Y.; Yang, Z. Hierarchical Nanoheterostructure of Tungsten Disulfide Nanoflowers Doped with Zinc Oxide Hollow Spheres: Benzene Gas Sensing Properties and First-Principles Study. *ACS Appl. Mater. Interfaces* **2019**, *11*, 31245–31256. [[CrossRef](#)]
53. Zhu, M.; Zhou, J.; Sun, P.; Peng, L.-M.; Zhang, Z. Analyzing Gamma-Ray Irradiation Effects on Carbon Nanotube Top-Gated Field-Effect Transistors. *ACS Appl. Mater. Interfaces* **2021**, *13*, 47756–47763. [[CrossRef](#)] [[PubMed](#)]
54. Zhang, J.; Liu, L.; Yang, Y.; Huang, Q.; Li, D.; Zeng, D. A review on two-dimensional materials for chemiresistive- and FET-type gas sensors. *Phys. Chem. Chem. Phys.* **2021**, *23*, 15420–15439. [[CrossRef](#)] [[PubMed](#)]
55. Kim, C.H.; Cho, I.T.; Shin, J.M.; Choi, K.B.; Lee, J.K.; Lee, J.H. A New Gas Sensor Based on MOSFET Having a Horizontal Floating-Gate. *IEEE Electron. Device Lett.* **2014**, *35*, 265–267. [[CrossRef](#)]
56. Liu, C.; Cao, Y.; Wang, B.; Zhang, Z.; Lin, Y.; Xu, L.; Yang, Y.; Jin, C.; Peng, L.-M.; Zhang, Z. Complementary Transistors Based on Aligned Semiconducting Carbon Nanotube Arrays. *ACS Nano* **2022**, *16*, 21482–21490. [[CrossRef](#)]
57. Qiu, C.; Zhang, Z.; Zhong, D.; Si, J.; Yang, Y.; Peng, L.-M. Carbon Nanotube Feedback-Gate Field-Effect Transistor: Suppressing Current Leakage and Increasing On/Off Ratio. *ACS Nano* **2015**, *9*, 969–977. [[CrossRef](#)] [[PubMed](#)]
58. Sun, Y.; Zhang, Y. Wafer-scale floating-gate field effect transistor sensor built on carbon nanotubes film for Ppb-level NO<sub>2</sub> detection. *Chem. Eng. J.* **2023**, *473*, 145480. [[CrossRef](#)]
59. Liang, Y.; Xiao, M.; Wu, D.; Lin, Y.; Liu, L.; He, J.; Zhang, G.; Peng, L.-M.; Zhang, Z. Wafer-Scale Uniform Carbon Nanotube Transistors for Ultrasensitive and Label-Free Detection of Disease Biomarkers. *ACS Nano* **2020**, *14*, 8866–8874. [[CrossRef](#)]

**Disclaimer/Publisher's Note:** The statements, opinions and data contained in all publications are solely those of the individual author(s) and contributor(s) and not of MDPI and/or the editor(s). MDPI and/or the editor(s) disclaim responsibility for any injury to people or property resulting from any ideas, methods, instructions or products referred to in the content.